Activation of CO_2 at the electrode-electrolyte interface by a co-adsorbed cation and an electric field

Journal:	*Physical Chemistry Chemical Physics*
Manuscript ID	CP-ART-12-2018-007807.R1
Article Type:	Paper
Date Submitted by the Author:	21-Mar-2019
Complete List of Authors:	Chernyshova, Irina; Columbia University, Earth and Environmental Engineering Ponnurangam, Sathish; University of Calgary, Chemical and Petroleum Engineering

Activation of CO_2 at the electrode-electrolyte interface by a co-adsorbed cation and an electric field

Irina V. Chernyshova,[a,b*] and Sathish Ponnurangam[c*†]

[a] Department of Earth and Environmental Engineering, Columbia University, New York, NY, United States

[b] Department of Geoscience and Petroleum, Norwegian University of Science and Technology, Trondheim, Norway

[c] Department of Chemical and Petroleum Engineering, University of Calgary, Calgary, Alberta, Canada

Abstract

Carboxylate $*CO_2^-$ has recently been identified as the first intermediate of the CO_2 electroreduction independent of the reaction pathway. However, on the fundamental level, the structural and electronic properties of $*CO_2^-$ remain poorly understood especially under the electrocatalytic conditions, which limits our capacity to rationally control the transformation of this reaction intermediate to CO or formate. To close this gap, we model using density functional theory (DFT) the interactions of $*CO_2^-$ with the copper Cu(111) surface and a co-adsorbed sodium cation in the electric double layer (EDL), as well as the effects of electrode potential on these interactions. We demonstrate that $*CO_2^-$ is activated by a co-adsorbed alkali cation most strongly when it forms with the cation a noncovalent bond (ion pair), where the cation is coordinated in the on-top position. The most stable structure of this ion pair with a sodium cation is hydration-shared. An external negative electric field not only enhances activation of $*CO_2^-$ but also tilts it in the $*CO_2^-$ plane, elongating the metal-C bond and contracting the metal-O bond. This tilting facilitates hydrogenation of the C atom and dissociation of the surface-coordinated C-O bond. Based on a detailed analysis of the projected density of states (pDOS), we interpret these findings in terms of electrostatic and chemical effects. The provided insights can help understand the relationship between properties of the catalytic system and its catalytic activity in the CO_2 conversion to CO and formate, and hence help develop new CO_2 electroreduction catalysts.

---

[*] Electronic supplementary information (ESI) is available

[†] **Corresponding authors**: Irina Chernyshova ic2228@columbia.edu and Sathish Ponnurangam sathish.ponnurangam@ucalgary.ca

1. Introduction

Electroreduction of abundant CO_2 to fuels is an emerging technology that can carve a unique niche as a complementary approach to store renewable energy.[1] This technology is also of interest from the viewpoint of exploration of Mars because it can supply fuels and carbonaceous chemicals during the Martian missions (CO_2 makes 95% of the Martian atmosphere). However, a viable catalyst of CO_2 electroreduction has not been found as of yet.[2] Hence, to expedite the progress, it is essential to improve the mechanistic understanding of this reaction.

Irrespective of the reaction pathway, CO_2 electroreduction starts with activation of CO_2 at the electrode-electrolyte interface. As recently demonstrated using operando surface enhanced Raman scattering (SERS) spectroscopy and density functional theory (DFT), this step produces a carboxylate intermediate $*CO_2^-$ (* underscores the adsorbed state)

$$* + CO_2 + e^- = *CO_2^- \quad (1)$$

which is coordinated to the metal surface with its C and O atoms, in a chair-like geometry (**Scheme 1**).[3]

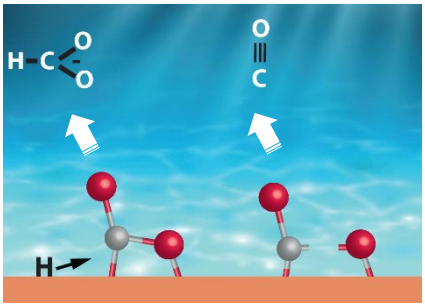

Scheme 1. Competing transformation of carboxylate $*CO_2^-$ at the electrode-aqueous electrolyte interface to formate via hydrogenation and carbon monoxide via dissociation.

The singular nature of the first intermediate suggests that the reaction branching in the second step toward either CO

$$*CO_2^- + e^- = CO + O^{2-} \quad (2)$$

or formate

$$*CO_2^- + e^- + H^+ = HCOO^- \quad (3)$$

is controlled by the propensity of $*CO_2^-$ to dissociate its C-O bond and be hydrogenated at its C atom, respectively (**Scheme 1**).[3] Competition between these two possible second steps is

expected to depend primarily on the geometric structure of $*CO_2^-$ which in turn depends on the properties of the catalytic system. However, this structure-property-selectivity relationship for CO_2 electroreduction is currently poorly understood.

This problem has motivated us to study in detail the interaction of $*CO_2^-$ with co-adsorbed alkali metal cations and the external electric field. Even though these effects have been addressed experimentally and theoretically,[3-13] most of the earlier studies have focused on the CO_2 activation from the gas phase. These studies have found that this reaction is promoted by a preadsorbed submonolayer of alkali metal atoms.[5-11] The promotion has been attributed to electrostatic effects combined with a decrease in the metal work function (enrichment of the metal surface with electron density).[5, 6, 8] Specifically, adsorbed alkali metal atoms are ionized (donate s electrons to the metal surface), which decreases the work function or increases Lewis basicity of the surface. In addition, the preadsorbed cations generate surface dipoles and electric fields beneficial for the formation of $*CO_2^-$ and its further dissociation and hydrogenation. In contrast, a DFT study in Ref.[4] has concluded that the effect of a co-adsorbed cation is purely electrostatic because the binding energy of $*CO_2^-$ does not depend on the work function of the supporting metal adjusted by pre-adsorbed Li or electrophilic halide atoms. It also has been shown theoretically that the electric field generated by co-adsorbed cations is highly localized, extending only up to ca. 5 Å from the center of the solvated cation.[4, 14]

However, except for Ref.,[3] the carboxylate-cation system has previously been modelled by placing a cation on the side of $*CO_2^-$, which is more relevant to the alkali metal-promoted CO_2 adsorption from the gas phase. At the electrode-electrolyte interface, apart from being co-adsorbed on the side, an alkali metal cation can also be coordinated on the top of $*CO_2^-$ through noncovalent (strong electrostatic) interactions such as ion-pairing. This additional interaction can explain the promoting effect of cation size on oxygen reduction reaction (ORR), hydrogen oxidation reaction (HOR), methanol oxidation, and chlorine oxidation on platinum.[15, 16] Hence, given that $*CO_2^-$ can form a hydration-shared ion pair with co-adsorbed Na^+,[3] noncovalent interactions can play an important role in the for CO_2 electroreduction, which needs to be explored.

The problem of the interaction of $*CO_2^-$ with co-adsorbed cations directly relates to the central effect in the electrocatalytic activation of CO_2—the effect of the externally applied electric field.[4, 14] Earlier DFT studies have shown that a negative electric field promotes this reaction, increasing the binding energy of $*CO_2^-$ by a purely electrostatic component.[4, 14] By the common

convention, the negative sign of the field means that the field is directed toward the metal surface and hence enriches it with electron density. However, the earlier theoretical studies have not reported how exactly the electric field modifies the chemical structure of $*CO_2^-$. This knowledge is important as it could help us understand which characteristics of the catalytic system control the selectivity of $*CO_2^-$ toward its transformation into either CO or formate.

Partial insight into the structural transformations of $*CO_2^-$ under applied electric field has recently been provided by operando SERS.[3] The spectra show that the metal-C and C-O bonds of $*CO_2^-$ on a Cu electrode are softened as the electrode potential is scanned in the negative direction, which has been explained by the electrochemical Stark effect. This effect presents a shift of the vibrational frequency of an adsorbed vibrating dipole with electrode potential which is commonly attributed to the purely electrostatic interactions of the vibrating dipole and the local electric field.[17] However, the effect of the electric field on the metal-O bond of $*CO_2^-$ remains unclear.

Finally, a conventional theoretical approach to understand the chemical bonding of the adsorbate is to analyze the charge redistribution upon its interaction with the surface, as well as the projected density of states (pDOS) of the resulting system.[13, 18, 19] Even though pDOS of CO_2 activated on transition metals has been calculated earlier,[12, 20-22] the frontier orbitals of $*CO_2^-$ have not been analyzed in detail, while their interpretation is confusing. For example, it has been concluded that the $*CO_2^-$ states that are closest to the Fermi level and hence dominate the chemical bonding descend from the O lone pairs,[20] the C-O π antibonding $2\pi^*$ orbital,[21, 23] or their mixture.[12]

Herein, we close the knowledge gaps about the structure and electronic properties of $*CO_2^-$ at the electrode-electrolyte interface and the effect of the electrode potential on this intermediate by using plane-wave DFT method and building upon our recent SERS and DFT results.[3] DFT modelling has already proven helpful in gaining microscopic insight into the CO_2 activation from gas phase across transition metals,[22, 24, 25] the promoting effect of alkali metal atoms on the CO_2 activation,[6, 26-28] as well as the effect of the external electric field.[12, 13, 27] As a catalyst, we chose copper because this metal is earth-abundant and famous for its unique capacity to convert CO_2 into C_{1+} products.[29] We limit our scope to the most stable Cu(111) facet and Na^+ as the electrolyte cation.

2. Simulation Methodology

DFT calculations were performed using a plane wave DFT code (The Vienna Ab initio Simulation Package, VASP-5.4.1).[30-32] A spin-polarized projector augmented wave (PAW) method was used for core and valence electron treatment along with a generalized gradient approximation (GGA) exchange-correlation (XC) functional (Perdew, Burke, and Ernzerhof, PBE).[33, 34] A 3×3 supercell of the Cu (111) surface was generated with three slabs of copper metal atoms and a vacuum gap of 25 Å in the direction perpendicular to the surface. The cutoff energy for the planewave basis set was fixed at 450 eV and the k-point mesh was generated using Monkhorst-Pack method (5×5×1 for surfaces). The Methfessel-Paxton scheme of order 1 was used for smearing the Fermi-level at a width of 0.1 eV. The geometry of the adsorbate was relaxed using conjugate-gradient algorithm. To reduce the computational cost, we kept positions of the Cu atoms frozen. In fact, when the topmost layer of Cu(111) in the (CO_2-$Na_{on\text{-}top}$)/Cu(111) system is allowed to relax, the calculation time increases by a factor of three, while changes in the CO_2 geometry are not significant, though the molecule is slightly less activated (**Table S1**, ESI). On this basis and given that the questions posed in this work require mostly qualitative analysis of the trends caused by the microenvironment and electric field, we ignore contributions of the surface relaxation to the effects of cation and electric field *CO_2^-. All systems reported are electrically neutral.

The optimized structures of *CO_2^- were obtained by placing a Na counter ion above or on the side of a linear CO_2 molecule, equidistantly from the CO_2 oxygen atoms. To understand the effect of an external electric field on the CO_2 activation, homogenous electric fields of +0.5 V/Å was applied in the z-direction (perpendicular to the Cu surface) while relaxing the geometry of *CO_2^-. Errors due to self-interaction of dipoles with periodic images in the x-y direction were corrected, whereas these interactions were minimized in the z-direction by creating a vacuum layer of 25 Å. All the slabs of Cu atoms were fixed spatially while and CO_2 and coadsorbed Na ion were relaxed such that the residual forces was less than 0.01 eV/Å.

The binding energy of CO_2 activated by Na, $\mathbf{\Delta E}$, is calculated as:

$$\mathbf{\Delta E} = \mathbf{E_{CO_2 + Na + Cu}} - \mathbf{E_{Cu}} - \mathbf{E_{Na}} - \mathbf{E_{CO_2}} \ , \qquad (4)$$

where $\mathbf{E_{Cu + CO_2 + Na}}$ is the electronic (DFT) energy of the relaxed *CO_2^- species on Cu with co-adsorbed Na^+ (either on-top or on-side of *CO_2^-), $\mathbf{E_{Cu}}$ is the energy of the clean Cu surface, and

E_{CO_2} is the energy of the relaxed configuration of a linear CO_2 molecule in vacuum, $\mathbf{E_{Na}}$ is the energy of either a Na atom in vacuum or a Na atom hydrated by 8 water molecules in vacuum.

As seen from eqn(4), binding energy $\mathbf{\Delta E}$ characterizes the interaction of both CO_2 and Na with the surface. Since the interaction of Na with the Cu surface is higher when Na is co-adsorbed on-side than on-top of CO_2, $\mathbf{\Delta E}$ is not indicative of the stabilization energy of CO_2 but rather of the whole system. Therefore, to remove the contribution of the electrostatic interaction of Na^+ with the surface, we also calculate the binding energies $\mathbf{\Delta E'}$ of CO_2 as

$$\mathbf{\Delta E' = E_{Cu + CO_2 + Na} - E_{Cu - Na} - E_{CO_2}}, \quad (5)$$

where all the terms are the same as in eq.(4), except for $\mathbf{E_{Cu - Na}}$. The latter is the energy of the interaction of Na with the Cu surface which is calculated as the energy of the Na-Cu system after removing CO_2 from the relaxed CO_2-Na-Cu system and freezing the Na position.

The partial charges on atoms are obtained by the Bader method using Henkelman's code whereby atoms are first separated by zero flux surfaces (plane of minimum charge density).[35, 36] The electronic charge densities enclosed inside these surfaces were integrated for each atom to calculate their partial charges (in excess/deficient of valence electrons). During the calculations, the total charge density ("core+valence" obtained from VASP using a fine FFT grid) was used to partition the charges and the vacuum charge was set to a low value of $1x10^{-5}|e|$. The Bader partitioning was performed using an ongrid algorithm. We use this method to understand the charge polarization in the system, bearing in mind that the absolute values of Bader charges are likely to be overestimated due to the intrinsic limitations of the GGA-level functionals to describe gaps between the highest occupied molecular orbitals (HOMO) and lowest unoccupied molecular orbitals (LUMO).[37-39]

The spatial re-distribution of the electronic charge density upon the CO_2 activation on Cu(111) by co-adsorbed Na is calculated by subtracting the charge densities of the $CO_2^{\bullet-}$…Na^+ ion pair, $\rho_{CO_2 + Na}$, (CO_2 reduced by a Na atom without the surface) and clean Cu(111), ρ_{Cu}, from the full final system, $\rho_{Cu + CO_2 + Na}$:

$$\rho_{redis} = \rho_{Cu + CO_2 + Na} - \rho_{Cu} - \rho_{CO_2 + Na}. \quad (6)$$

The atomic positions of the clean Cu(111) surface and of the $CO_2^{\bullet-}$…Na^+ ion pair are taken to be the same as those of the (CO_2+Na)/Cu(111) relaxed system. Eqn. (6) highlights changes in the electronic structure of the CO_2 moiety of $CO_2^{\bullet-}$ upon its adsorption on the Cu surface.

The electric field distribution created by a sodium cation and the Cu(111) surface at the interface around $*CO_2^-$ is calculated following the methodology reported in Refs.[14, 40] Single point energy calculations are performed on the whole environment without $*CO_2^-$ (obtained by removing the adsorbed CO_2 from energy minimized configuration of the full system), as well for the individual components of the environment, viz., Cu(111) alone, and Na cation (or hydrated cation) alone. The Bader charges are calculated from these runs and are further used for determining electric field distribution. Specifically, electrostatic potential is calculated along the lines perpendicular to the surface (parallel to z axis) and passing through the surface-coordinated carbon and oxygen atoms of $*CO_2^-$ at 0.25 Å interval along this line:

$$\mathrm{V_z} = \mathrm{V_{env,z}} - (\mathrm{V_{Cu,z}} + \mathrm{V_{Na,z}}(\mathrm{or\ V_{Na+8H2O,z}})), \tag{7}$$

where, $\mathrm{V_{env,z}}$ $\mathrm{V_{Cu,z}}$, and $\mathrm{V_{Na,z}}$ are electrostatic potentials of the environment (full system without adsorbed CO_2), Cu(111) surface alone, and Na cation (or hydrated Na) alone, respectively). The electric field (strength) is calculated as negative gradient of potential along the z direction starting from the vacuum side and approaching the surface as:

$$\overrightarrow{\Delta \mathrm{E}}_{\frac{z_2+z_1}{2}} = -\frac{(\mathrm{V_{z_2}} - \mathrm{V_{z_1}})}{z_2 - z_1}\ . \tag{8}$$

It is known that the implementation of an external electrical field in a periodic system can lead to a leakage of electrons between the system (surfaces, molecules, etc.) and the external electrodes that are used to create the electric field.[41] We verified that no such artificial charge transfer by ensuring that the vacuum charge obtained through Bader analysis is close to zero.

To clarify the electronic picture of the bonding between CO_2 and Cu(111), we calculated the total density of states (DOS) and DOS projected on molecular orbitals of specified atoms (pDOS). For this, we performed single point energy calculations using the same method (PAW) and exchange-correlation functional (PBE) as well as the k-point grid (5 × 5 × 1 Monkhorst–Pack) but under more refined conditions (plane-wave energy cutoff of 650 eV and tight electronic convergence criteria of 10^{-6} eV). To identify the hybrid molecular orbital that dominate each pDOS band, we calculated the decomposed charge density for each band and visualize it as the 3D electron density plot using VESTA.[42] To avoid the ambiguity in interpretation of pDOS bands, we calculated the electron density isosurface (band-decomposed charge density) for each band, which visualizes the shape of the corresponding hybridized orbital.

3. Results

In our models, CO_2 is reduced to carboxylate $*CO_2^-$ on the Cu(111) surface negatively charged by a co-adsorbed Na atom. The resulting Na^+ cation simulates the local environment of $*CO_2^-$ at the negatively charged electrode-electrolyte interface. To understand the chemical bonding between $*CO_2^-$ and the Cu(111) surface, we compare the relaxed structures of $*CO_2^-$ with a free $CO_2^{\bullet-}$ anion radical rather than a linear CO_2 molecule because CO_2 is more strongly activated in $*CO_2^-$ than in the free radical. Therefore, the comparison with $CO_2^{\bullet-}$ helps us understand contribution of the surface to the CO_2 activation beyond electron transfer.

We interpret the chemical bonding of $*CO_2^-$ with the Cu(111) surface mostly within the classical (Blyholder-like) model of the molecule-surface interactions.[18, 19] These interactions include the stabilizing chemical bonding through electron back-donation to and synergetic donation from the adsorbate, combined with electrostatic polarization of hybridized molecular and metal states, while the destabilization is underpinned by the Pauli repulsion of the closed shell electrons of the adsorbate by electrons of the adsorbent surface. In addition, we find rehybridization of the d metal and 1π and $2\pi^*$ molecular states, which suggests that the interactions are more complex than the framework of the classical model.

3.1. The local environment of $*CO_2^-$ at the electrode-electrolyte interface: Interaction with alkali metal cation

In this section, we show that a Na^+ cation co-adsorbed in the on-top position activates CO_2 more strongly than the Na^+ cation co-adsorbed on the side. We explain the promoting effects by an increase in the local electric field acting on CO_2. When the on-top Na^+ cation is hydrated, the $*CO_2^-$…Na^+ system is stabilized as a hydration-shared ion pair.

In the first DFT model, we place a Na atom on the top of the carbon atom of a CO_2 molecule physisorbed on Cu(111) (**Figure S1**). In the relaxed system (**Figure 1b**), dubbed as (CO_2-$Na_{on\ top}$) hereafter, Na stays on top, while CO_2 is activated as carboxylate $*CO_2^-$ in a chair-like geometry coordinated to the surface with the C and O atoms. Importantly, CO_2 is activated significantly more strongly in (CO_2-$Na_{on\ top}$) than in $CO_2^{\bullet-}$ (the latter was simulated as a CO_2-Na pair in vacuum) (**Figure 1a** and **Table 1**). In fact, the O-C-O bond angle of 119.5° of $*CO_2^-$ is significantly smaller than 134° of $CO_2^{\bullet-}$. The C-O bond of $*CO_2^-$ coordinated to the surface is longer (1.35 Å) than the C-O bonds of $CO_2^{\bullet-}$ (1.25 Å), the other C-O bond of $*CO_2^-$ remaining the same (1.25 Å). This result is consistent with a lower experimental frequency observed for the

asymmetric C-O stretching vibration of $*CO_2^-$ at the Cu-electrolyte interface, which is in the 1540-1510 cm^{-1} range,[3] as compared to 1570-1650 cm^{-1} reported for CO_2-alkali metal (C_{2v}) adducts in noble gas matrices.[43, 44] Even though this vibration is dominated by the C-O stretching of the non-coordinated C-O bond of $*CO_2^-$, it has an admixture of the C-O stretching vibration of the surface-coordinated C-O bond.[3]

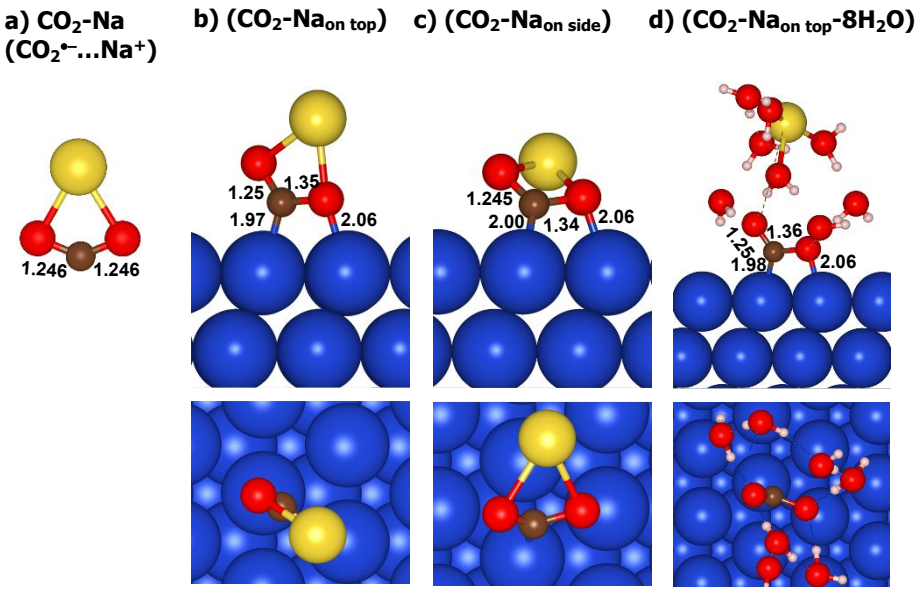

Figure 1. Side and top views of the relaxed structure of CO_2 activated by Na (**a**) in vacuum as $CO_2^{\bullet-}$ and (**b-d**) on Cu(111) (**b**) Na on the CO_2 top, (**c**) Na on the CO_2 side, (**d**) Na hydrated by 8 water molecules on top (Na is removed from the top view). The numbers show bond lengths in Å. Top panel=side view. Bottom panel=top view. Atom colors: dark blue – Cu, red – oxygen, brown – carbon, yellow – sodium.

Table 1. Geometry, Bader charges, and binding energies of relaxed structures of weakly physisorbed CO_2, free $CO_2^{\bullet-}$ radical (CO_2-Na), and CO_2 activated on Cu(111) in the presence of Na

	CO_2/ Cu(111)	$CO_2^{\bullet-}$	(CO_2-Na_{side})	(CO_2-Na_{top})	(CO_2-Na_{on-top} +8H_2O)
			Bader charge (|e|)		
C	1.661	1.541	0.635	0.628	-
O_1	-0.927	-1.216	-0.790	-0.850	-
O_2(Cu)	-0.875	-1.137	-0.857	-0.860	-
Total on CO_2	-0.141	-0.811	-1.012	-1.082	-
Cu(C)	-	-	0.142	0.149	-
Cu(O_2)	-	-	0.239	0.244	-
Na^+	-	0.812	0.658	0.756	-

Total Charge	0.002	0.001	0.001	0.001	-
			Bond length (Å)		
C–O_1	1.17	1.246	1.245	1.248	1.249
C–O_2	1.17	1.246	1.337	1.351	1.357
C–Cu	3.25	NA	2.003	1.973	1.975
O_2–Cu	3.55	NA	2.063	2.058	2.060
Cu…Na	NA	NA	4.286	4.502	6.811
C...Na	NA	2.445	2.541	2.547	4.864
O_1…Na	NA	2.268	2.364	2.229	4.012
			O-C-O angle (°)		
	180.0	133.9	121.2	119.5	119.1
			Binding energy (eV)*		
	0.026	NA	–1.64	–1.51	–2.16

*) Binding energy is calculated using eqn (4). These values characterize the interaction of both CO_2 and Na with the surface. Hence, they cannot be used to compare the interaction of only CO_2 with the surface. We report these values to show that in the presence of Na the carboxylate formation on Cu(111) is highly exergonic, while hydration significantly stabilizes the system. O_1=O atom of $*CO_2^-$ pointing out of the surface. O_2=O atom of $*CO_2^-$ coordinated to the surface.

The strong promoting effect of Cu(111) on the CO_2 activation is supported by the Bader charge analysis (**Table 1**). Adsorbed carboxylate $*CO_2^-$ in (CO_2-$Na_{on\ top}$) has a total negative charge of –1.01|e|, which is significantly larger than –0.81|e| on $CO_2^{\bullet-}$. As compared to $CO_2^{\bullet-}$, the C atom of $*CO_2^-$ gains a negative charge of –0.91|e|. Noteworthy is that both the O atoms of $*CO_2^-$ are significantly less negatively charged than those of $CO_2^{\bullet-}$. Based on the electronic structure of $*CO_2^-$ (see below), this effect can be accounted for by the formation of a dative bond between the O lone pair and the coordinating Cu atom. The dative bond presents a highly polar coordination bond between an acceptor (a Lewis acid) and a donor of an electron pair (a Lewis base). In contrast, the covalent bond is a coordination bond in which each coordinated atoms provides one electron to the pair to be shared.

Another important result of the Bader analysis is that the Cu atoms coordinating the C and O atoms of $*CO_2^-$ are positively charged by +0.14|e| and +0.24|e|, respectively. This can be accounted for by several effects including: i) the image charge effect[45] which screens the negative charge on $*CO_2^-$; ii) the polarization of Cu sp and d electrons to minimize the repulsive (Pauli) interactions, and iii) back-donation of Cu electron density into the LUMO of CO_2 upon formation of the covalent bond between $*CO_2^-$ and the surface (see below for more detail). Because of the charge loss on the O atoms, the charge transferred to the C atom of the CO_2 molecule is a more

straightforward characteristics of the CO_2 activation than the net charge transferred to CO_2. Hence, in the following, along with the O-C-O angle and the C-O bond lengths, we use the charge gained by the C atom as a primary characteristics of CO_2 activation.

In the next DFT model, which is dubbed as (CO_2-$Na_{on\ side}$), we place a Na atom on the side of the carbon atom of a CO_2 molecule physisorbed on Cu(111) as in Refs.[4, 6] In this case, $*CO_2^-$ is also stabilized in the chair geometry but its plane is tilted toward the co-adsorbed Na^+ cation (**Figure 1c**). Importantly, the CO_2 activation in (CO_2-$Na_{on\ side}$) is significantly weaker than in (CO_2-$Na_{on\ top}$). Specifically, CO_2 in (CO_2-$Na_{on\ side}$) has a larger O-C-O bond angle of 121.2° (as compared to 119.5°) (**Table 1**). The coordinated C-O bond of 1.337 Å of $*CO_2^-$ in (CO_2-$Na_{on\ side}$) is shorter (as compared to 1.357 Å), though its Cu-O bond is almost the same. The stronger stabilization of CO_2 in (CO_2-$Na_{on\ top}$) than in (CO_2-$Na_{on\ side}$) is also evidenced by the binding energy of CO_2 calculated using eqn.(5), which is −0.75 and +0.06 eV, respectively. The Bader charge analysis further supports this conclusion. As compared to (CO_2-$Na_{on\ top}$), the C atom of $*CO_2^-$ loses some electron density (becomes slightly less positive), while the total negative charge on CO_2 increases from −1.02|e| to −1.08|e|.

The stronger activation of CO_2 by the Na^+ cation coordinated on-top as compared to on-side is explained by a much stronger negative local electric field acting on $*CO_2^-$ in the former case. As seen from **Figure 2,** and can be expected from the elemental electrostatics argument, the electric fields acting on the C and surface-coordinated O atoms of (CO_2-$Na_{on\ top}$) are by a factor of 2 higher than in the case of (CO_2-$Na_{on\ side}$).

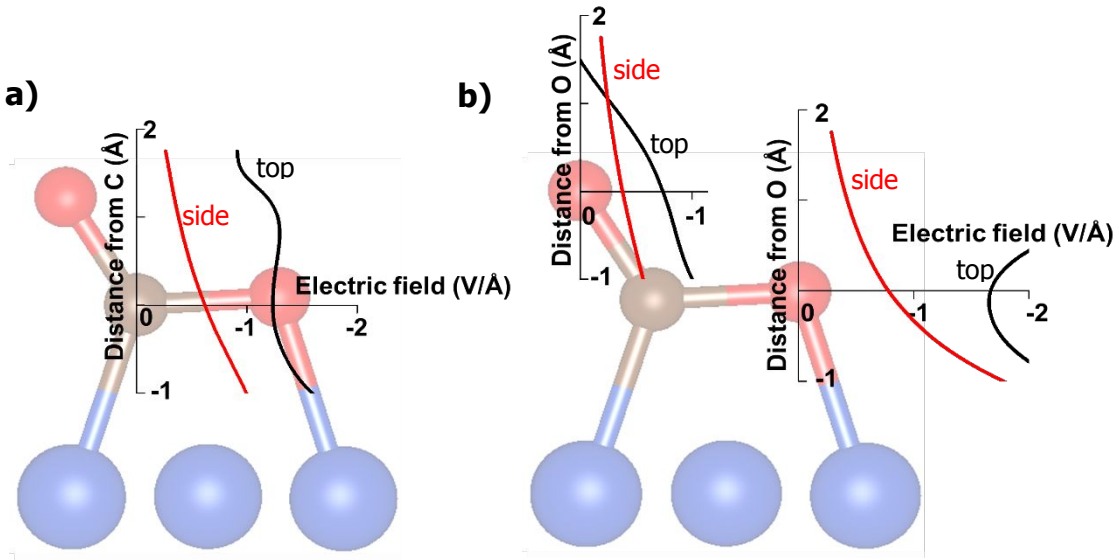

Figure 2. DFT-predicted distribution of electric field at (**a**) C and (**b**) O atoms of $*CO_2^-$ stabilized on Cu(111) by Na^+ in (**red**) on-side and (**black**) on-top position.

In ther next step, we exlore the effect of hydration on the interaction of $*CO_2^-$ with Na^+ in the EDL. By analogy with the ion pairing of carboxylate groups in solution and at the protein-solution interface,[46, 47] hydration is expected to control the promoting effect of the cation on $*CO_2^-$. However, currently the hydration state of $*CO_2^-$ in the electric double layer is barely characterized. To model the hydration, we first have relaxed a Na^+ cation hydrated by eight water molecules in vacuum and then place the hydrated cation on the top of the physisorbed linear CO_2 molecule (**Figure S1**). After relaxation, the system, which is labelled as (CO_2-$Na_{on\text{-}top}$+8H_2O), is stabilized as a hydration-shared ion pair, where $*CO_2^-$ interacts with the on-top Na^+ cation through the adjacent hydrogen bonded water molecules (**Figure 1d**). Within calculation error, the geometries of carboxylate in (CO_2-$Na_{on\text{-}top}$+8H_2O) and (CO_2-$Na_{on\ top}$) are similar (**Table 1**). This result may suggest that the water molecules shared by $*CO_2^-$ and Na^+ are so strongly polarized that they generate similar local electric fields around $*CO_2^-$ as in the non-hydrated Na^+ cation itself. However, it requires further verification using a more extensive theoretical model.

Importantly, within its limitations, our theoretical model predicts that hydration-shared is the thermodinamically most stable configuration of the $*CO_2^-$…Na^+ ion pair in the EDL. In fact, when we attempted to model the alternative configuration—contact ion pair—it was destabilized toward the hydration-shared one (**Figure S2**). It follows that the co-adsorbed Na^+ cation prefers to share its hydration shell with $*CO_2^-$ rather than to interact electrostatically directly.

Thus, on a negatively charged Cu(111) surface, CO_2 is activated more strongly than in $CO_2^{\bullet-}$ due to the additional chemical interactions of $*CO_2^-$ with the Cu surface and the stabilizing electrostatic effects at the interface. The configuration in which $*CO_2^-$ is most stable presents an ionic pair where the cation co-adsorbed in the on-top position. In this configuration, the co-adsorbed cation imposes on $*CO_2^-$ a negative electric field by a factor of ca. 2 stronger than in the on-side configuration, while the binding energy of CO_2 is by –0.8 eV more negative. In the presence of hydrating water molecules, the hydration-shared structure of the ion pair is more stable than contact one. The above findings suggest that a critical role of the interaction of both $*CO_2^-$ and electrolyte cation with their hydrating water molecules in the stabilization of the ion pair.

3.2. Electronic structure of $*CO_2^-$

3.2.1. Charge redistribution. Before analyzing the charge redistribution upon the $*CO_2^-$ formation we recall that the orbital responsible for the reduction of CO_2 is its LUMO. It presents the in-plane component of the doubly degenerate $2\pi^*$ C-O antibonding orbital (**Figure S3b**).[8, 48] In $CO_2^{\bullet-}$, it changes the symmetry and is labeled as $6a_1$ (**Figure S3a**). In agreement with its antibonding character, $6a_1$ has nodes between the C and O atoms, while its main lobe is located on the C atom (we neglect the interaction of this orbital with Na^+) (**Figure 3c,d**). The pDOS analysis shows that $6a_1$ of $CO_2^{\bullet-}$ is composed of 34% C 2p, 9% C 2s, and 52% O 2p (**Figure S3**).

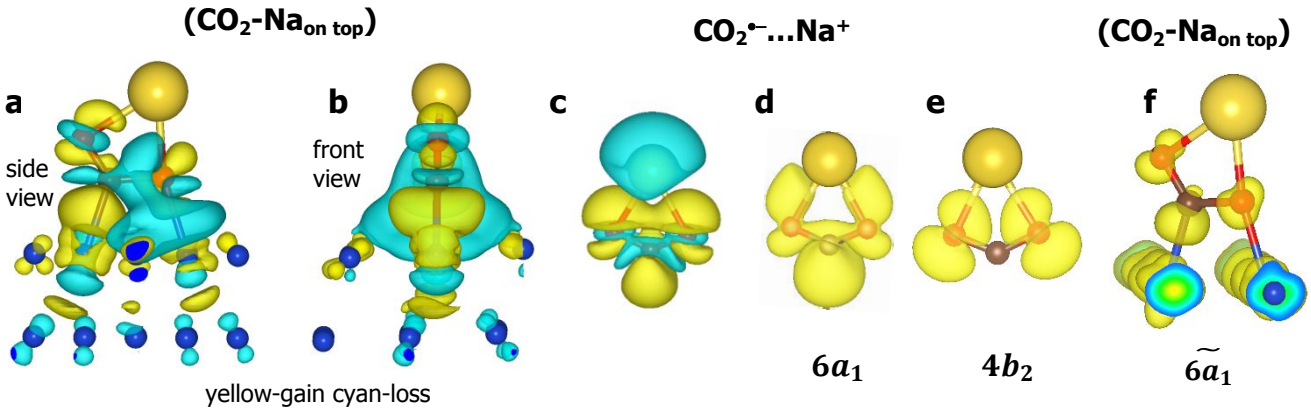

Figure 3. Charge redistribution ρ_{redis} (yellow-gain, cyan-loss) upon formation of (**a,b**) (CO_2-$Na_{on\ top}$) calculated using eqn. (6), (**c**) $CO_2^{\bullet-}$ anion radical (simulated as $CO_2^{\bullet-}$...Na^+ ion pair). (**d,e,f**) Electron density isosurfaces of the frontier (**d**) $6a_1$ and (**e**) $4b_2$ orbitals of $CO_2^{\bullet-}$ and (**f**) $\widetilde{6a_1}$ of (CO_2-$Na_{on\ top}$).

3.2.1. Charge redistribution. Before analyzing the charge redistribution upon the $*CO_2^-$ formation we recall that the orbital responsible for the reduction of CO_2 is its LUMO. It presents the in-plane component of the doubly degenerate $2\pi^*$ C-O antibonding orbital (**Figure S3b**).[8, 48] In $CO_2^{\bullet-}$, it changes the symmetry and is labeled as $6a_1$ (**Figure S3a**). In agreement with its antibonding character, $6a_1$ has nodes between the C and O atoms, while its main lobe is located on the C atom (we neglect the interaction of this orbital with Na^+) (**Figure 3c,d**). The pDOS analysis shows that $6a_1$ of $CO_2^{\bullet-}$ is composed of 34% C 2p, 9% C 2s, and 52% O 2p (**Figure S3**).

The charge redistribution ρ_{redis} of (CO_2-$Na_{on\ top}$), which was calculated using eqn.(6) (**Figure 3a,b**), reveals that bonding of $CO_2^{\bullet-}$ to Cu(111) is primarily governed by further population of its $6a_1$ orbital. Indeed, ρ_{redis} within the CO_2 moiety of (CO_2-$Na_{on\ top}$) qualitatively resembles ρ_{redis} observed when CO_2 is reduced by Na alone (**Figure 3c**). Electron density is depleted within the C-O bonds and gained on the C and O atoms where lobes the $6a_1$ are

expected. This picture suggests a charge flow from the Cu(111) surface to the $6a_1$ orbital of $CO_2^{\bullet-}$, which is confirmed by the Bader analysis below. It also shows that the $\widetilde{6a_1}$ orbital (the tilde labels the hybridized state) is antibonding with respect to the C-O π bonds but bonding with respect to the C-Cu and O-Cu bonds of $*CO_2^-$.

The electron density gain is most pronounced on the C lobe of $*CO_2^-$ (**Figure 3a**). It fills up the entire region between the C and Cu atoms, which indicates $CO_2^{\bullet-}$ forms a strong covalent Cu-C bond with the Cu surface.[49] The density gain along the Cu-O bond is less pronounced and polarized off the bond center, suggesting that the Cu-O bond is less covalent (more ionic) as compared to the Cu-C bond, which is confirmed by the pDOS analysis below.

Another feature of (CO_2-$Na_{on\ top}$) is bi-directional charge redistribution on its coordinating Cu atoms (**Figure 3a**): Charge is depleted on the d_{z2} (axial) states and gained on the d_π (d_{xz} or/and d_{yz}) states. This effect can be interpreted in terms of donation and back-donation of the d electron density.[19, 50-52] Specifically, the coordinating Cu atoms back-donate d_{z2} density to the $6a_1$ orbital of $CO_2^{\bullet-}$, which underpins the formation of the covalent Cu-C and Cu-O bonds. Simultaneously, the d_π states accept some electron density from $CO_2^{\bullet-}$ to minimize the Pauli repulsion. Pauli repulsion presents the short-range repulsion between the overlapped occupied states in the adsorbate and the metal (also called repulsive σ interactions) due to the Pauli exclusion (quantum mechanical) principle.[45, 49] The stronger the overlap, the larger the repulsion.

Another important effect that partially mitigates the Pauli repulsion is the 'pillow'-like, or 'push-back' polarization of the metal sp density around $*CO_2^-$.[53] As seen from **Figure 3a,b**, there is a highly delocalized electron density loss just above and around the Cu atom coordinating the O atom. In addition, Cu sp density is depleted across several Cu atomic layers beneath $*CO_2^-$. Finally, there is a typical push-back of electron density around $*CO_2^-$: Electron density is accumulated on the topmost Cu atoms that surround $*CO_2^-$ and just below the coordinating Cu atoms due to the push back out of their space. The loss of electron density on the Cu atoms electrostatically stabilizes the adsorbed carboxylate anion.

Thus, $CO_2^{\bullet-}$ is stabilized on the metal surface features by a strong covalent metal-C bond, a more ionic metal-O bond, and strong electrostatic interactions, while destabilized by the Pauli repulsion.

3.2.2. Projected density of states (pDOS). We analyze pDOS at the binding energies below the Fermi level from 0 to −10 eV because these states are derived from the outer valence orbitals of $CO_2^{\bullet-}$ which directly interact with the surface as evidenced by their pronounced

presence in the d and sp pDOS of Cu(111) (**Figures 4** and **S4**, respectively). For the simplicity sake, we limit our analysis to (CO_2-$Na_{on\ top}$) rather than to the more stable (CO_2-Na+8H_2O).

First of all, even though $*CO_2^-$ can be viewed as adsorbed $CO_2^{\bullet-}$, this species lacks the radical properties due to its interaction with metal electrons (**Figure S5**). The spin coupling upon the $*CO_2^-$ formation is discussed by Hedström et al.[54]

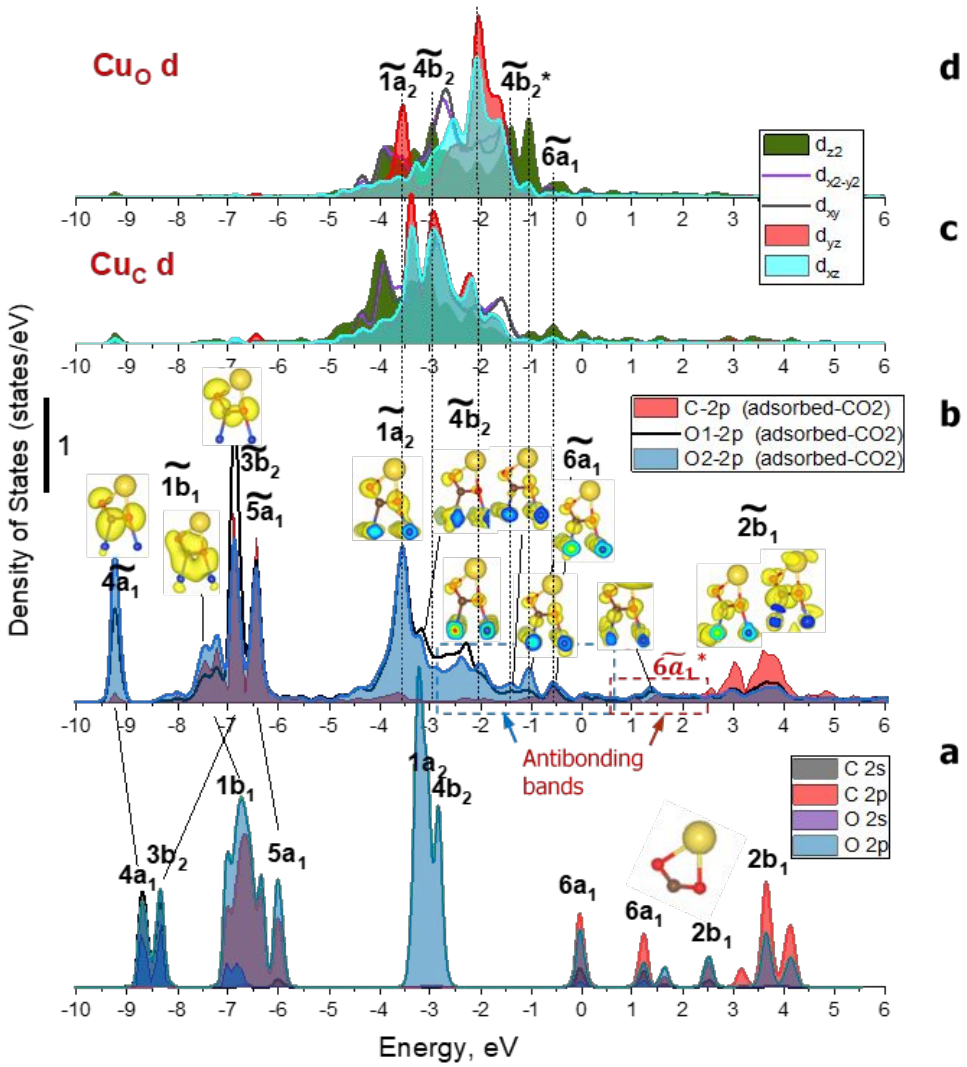

Figure 4. Projected DOS (**a**) O 2s, C 2s, O 2p, and C 2p of free $CO_2^{\bullet-}$ anion radical modelled as CO_2-Na ion pair, (**b**) O 2p and C 2p, (**c**) Cu d of the Cu atom coordinating the C atom of $*CO_2^-$ and (**d**) Cu d of the Cu atom coordinating the O atom of $*CO_2^-$ in (CO_2-$Na_{on\ top}$)/Cu(111) (**Figure 1b**). Panel (**b**) includes graphs that visualize the spatial distribution of the electron density of the hybrid molecular states of $*CO_2^-$. Dashed line boxes indicate approximate positions of the antibonding frontier orbitals of $*CO_2^-$.

Second of all, the O 2p and C 2p pDOS of (CO_2-$Na_{on\ top}$) (**Figure 4b**) confirm that the $6a_1$ orbital plays the key role in the bonding of $*CO_2^-$ with the metal surface. In free radical $CO_2^{\bullet-}$, this orbital is pinned at the Fermi level (**Figure 4a**), which is explained by its half occupancy. Hybridization with the Cu d states splits $6a_1$ into the $\widetilde{6a_1}$ bonding and antibonding bands which overlap with the antibonding band of the hybridized O lone pair states (see below) (**Figure 4b**). The $\widetilde{6a_1}$ states are distinguished from the O lone pair states by the presence of the C 2p pDOS in the former.

The antibonding part of $\widetilde{6a_1}$, $\widetilde{6a_1}^*$, occupies the energy states from +0.7 to ca. +2.0 eV and therefore is empty. The bonding part spreads from −1.4 eV up to ca. +0.7 eV, the main resonance being at −0.57 eV. This resonance state is composed of 13% C 2p, 4% C 2s, and 32% O 2p, 30% Cu d_{z2}, and 20 % Cu 4p. The comparable contributions from the molecular and metal states reflects the fact that $\widetilde{6a_1}$ is responsible for the covalent bonding of $*CO_2^-$ with the Cu surface through the backdonation mechanism (see above). Given that the total stabilization energy of (CO_2-$Na_{on\ top}$) is −1.51 eV (**Table 1**), the covalent bonding of $*CO_2^-$ with the Cu surface contributes only ca. 40% of the total stabilization energy. The remaining stabilization comes from the dative bonding within the metal-O bond of $*CO_2^-$ (see below) and the electrostatic (ionic) interactions. Because the $\widetilde{6a_1}$ orbital crosses the Fermi level with the bonding, stabilization of this orbital will result in the enhancement of the covalent bonding of $*CO_2^-$ with the Cu surface.

States in the energy region from ca.−5.0 eV and up (**Figure 4b**) are derived from the perpendicular ($1a_2$) and in-plane ($4b_2$) O lone orbitals, which are HOMO-1 and HOMO of $CO_2^{\bullet-}$, respectively (**Figure S3**). These orbitals descend from the doubly degenerate $1\pi_g$ lone pairs of CO_2 and hence are purely O-centered. As seen from **Figures 4** and **S4**, these orbitals mix with delocalized Cu p states and the localized Cu d-band, which broadens and splits them into several bands. These include the bonding and antibonding combinations centered on the coordinated and non-coordinated O atoms of $*CO_2^-$. The bonding cluster is relatively narrow. It has three main resonances at ca. −3.55, −3.25, and −2.9 eV which are assigned to $\widetilde{1a_2}$, $\widetilde{4b_2}$ centered on the non-coordinated O atom, and $\widetilde{4b_2}$ centered on the coordinated O atom, respectively.

The $\widetilde{1a_2}$ orbital originates from the perpendicular O lone pair of $CO_2^{\bullet-}$. Due to the geometry constraints, it mixes only with Cu d_{yz} states, as follows from a distinct common state at −3.55 eV in $\widetilde{1a_2}$ and the Cu d_{yz} band of the Cu atom coordinating the O atom of $*CO_2^-$ (**Figures 4d** and **S6b**). The antibonding band $\widetilde{1a_2}^*$ is likely to be fully occupied (we do not trace in the electron

density isosurfaces around the Fermi level the $1\widetilde{a}_2$ features). This means the $1a_2$-d_{yz} interaction is dominated by a combination of Pauli repulsion.

The upper lying $4\widetilde{b}_2$ orbital originates from the in-plane O lone pair ($4b_2$) molecular orbitals of $CO_2^{\bullet-}$. It strongly hybridizes with the Cu d_{z2} states, as follows from the $4\widetilde{b}_2$ resonance at −2.9 eV and the $4\widetilde{b}_2^*$ resonances at −1.4 and −1.1 eV in the Cu d_{z2} band of the Cu atom coordinating the O atom of $*CO_2^-$. The antibonding band $4\widetilde{b}_2^*$ spreads from ca. −2.7 eV toward the Fermi level where it degenerates with $6\widetilde{a}_1$ (marked by a dash-line box in **Figure 4b**). Based on the results of Crystal Orbital Hamilton population analysis of a less activated $*CO_2^-$ species formed spontaneously on transition-metal doped Cu(111) and Cu(100) surfaces,[23] it is likely that the tail of the $4\widetilde{b}_2^*$ states crosses the Fermi level. Depopulated antibonding states signify that the interaction of the $4b_2$ orbital of $CO_2^{\bullet-}$ with the Cu surface is bonding. Hence, in addition to the electrostatic and covalent interactions, $*CO_2^-$ is stabilized through the dative bonding channel which involves its in-plane O lone pair. The formation of the dative bond explains the decrease in electron density on the O atoms of $CO_2^{\bullet-}$ upon its interaction with Cu(111) (**Table 1**).

Taking into account that the d shell of Cu is almost fully occupied ($d^{9.6}$), one could expect that donation of electron density from the parallel O lone-pair molecular orbital $4b_2$ of $CO_2^{\bullet-}$ into d_{z2} Cu states (dative bonding) would be very limited as in the case of the dative bonding between the O lone pair of adsorbed water and a Cu surface.[50, 55] However, in the case for $*CO_2^-$ the dative bonding is formed in concert with the covalent bonding thorough the $6a_1$ channel (see above). The latter includes back-donation of d_{z2} electron density into the $6a_1$ orbital, which empties the d_{z2} states on both the Cu atoms coordinating $*CO_2^-$. Hence, the d_{z2}-$4b_2$ dative bonding is synergetic with the d_{z2}-$6a_1$ covalent bonding, suggesting the $6a_1$-$4b_2$ rehybridization. This result is important because it means that electron enrichment of the Cu surface will destabilize the Cu-O bond by the electrostatic and Pauli repulsion but stabilize chemically, as demonstrated by the effect of the external electric field on pDOS (see below).

At higher binding energies (−6 - −10 eV), pDOS is represented by states that originate from two σ lone pairs ($4a_1$ on C and $3b_2$ on O) of $CO_2^{\bullet-}$, as well as from the occupied perpendicular and in-plane π C-O bonding orbitals ($1b_1$ and $5a_1$, respectively) (**Figure 4a,b**). The $3b_2$ lone pair practically does not mix with the Cu states due to its unfavorable spatial geometry. As a result, this orbital is destabilized by the Cu surface due to Pauli repulsion. The remaining three orbitals ($4a_1$, $1b_1$ and $5a_1$) are stabilized. The former two mix with the Cu s states, while the in-plane π

C-O bonding orbital interacts with Cu p states. All the three orbitals also mix with the Cu d_{z2} and d_{π} states (**Figure S6**). However, these three orbitals interact with the metal valence band weakly, as seen from their weakly perturbed widths. On this basis, given the deep position of these three orbitals,[56] we conclude that these orbitals contribute to the CO_2-Cu interaction mostly by a Pauli repulsion.

Finally, pDOS exhibits the antibonding $2b_1$ states of $CO_2^{\bullet-}$, which are derived from the perpendicular component of $2\pi^*$ (**Figure S3**). These states lay above the Fermi level (**Figure 4**) and hence do not participate in the adsorption.

Additional details about the interaction of CO_2 with Cu are provided by the analysis of the hybridized d_{z2} and d_{π} states of the Cu atoms coordinating the C and O atom of CO_2 (**Figure S6** and text in ESI). This analysis confirms that the most strongly interacting with $*CO_2^-$ are the Cu d_{z2} states of the Cu atom that coordinates the C atom of CO_2. In addition, Cu d pDOS demonstrate the d-d rehybridization between the d_{z2} and d_{π} states of the C- and O-coordinating Cu. This effect depopulates the d states overlapped with the close-shell orbitals into the available empty states to mitigate the Pauli repulsion, as a complementary mechanism to the "push-back" polarization of metal free electrons.[50, 57]

Thus, $*CO_2^-$ forms with a Cu surface a covalent bond through the $6\widetilde{a}_1$ states derived from LUMO. The remaining contributions are due to the dative Cu-O bonding through the $4\widetilde{b}_2$ (HOMO) channel and electrostatic effects (ionic bonding of the molecular orbitals with positively charged coordinating Cu atoms). The destabilization comes from the Pauli repulsion of the σ lone pair on C ($4\widetilde{a}_1$), perpendicular π O-lone pair ($1\widetilde{a}_2$), and C-O π electrons ($1\widetilde{b}_1$ and $5\widetilde{a}_1$). Even though the net contribution of the covalent bonding to the total stabilization energy of $*CO_2^-$ is low (~40%), the interaction of the carboxylate with the Cu(111) surface is strong as manifested by the rehybridization within the individual sets of the molecular and metal states.

3.3. Effect of external uniform electric field

To model the effect of electric field on $*CO_2^-$, we apply different uniform electric fields to (CO_2-$Na_{on\ top}$) (**Figure 1a**). However, among electric fields of +1.0, +0.5, −0.5, and −1.0 V/Å tested, calculations converge only at a positive electric field of +0.5 V/Å.

As expected, CO_2 is more activated at a zero external electric field as compared to +0.5 V/Å (**Figure 5** and **Table 2**). This effect is manifested by a decrease in the O-C-O bond angle and softening of the C-O bonds (especially, the surface coordinated one) of $*CO_2^-$. The Na^+ cation

approaches $*CO_2^-$ and the surface closer, in agreement with the expected shrinking of the EDL width. The total negative charge on $*CO_2^-$ increases from –1.03|e| to –1.08|e|. Of a particular interest is that the Cu-C bond of $*CO_2^-$ is slightly lengthened, while the Cu-O bond is contracted at 0 V/Å as compared to +0.5 V/Å. These structural changes suggest that carboxylate becomes more susceptible to both the dissociation of its surface coordinated C-O bond and the hydrogenation of its C atom (**Scheme 1**).

The theoretically predicted elongation of the Cu-C and C-O bonds of $*CO_2^-$ is in agreement with the SERS results.[3] This effect has earlier been attributed to the Stark effect,[3] though it can also be accounted by the chemical effect (see below). At the same time, the Stark effect cannot explain the predicted contraction of the Cu-O bond. The Cu-O dipole is co-parallel to the negative electric field, which would result in the elongation of this bond by the field, which is opposite to what is predicted.

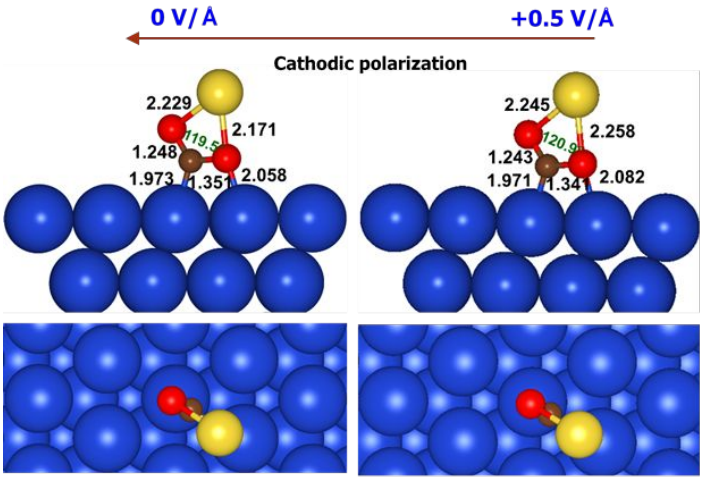

Figure 5. Effect of external electric field on (CO_2-$Na_{on\ top}$). Bond lengths and angles are in Å and degrees, respectively. Atom colors: dark blue – Cu, red – oxygen, brown – carbon, yellow – sodium.

Table 2. Effect of electric field on the geometry and Bader charges of CO_2 adsorbed on Cu (111) with Na^+ in the on-top position (**Figure 5**)

Electric Field	+0.5 V/Å	0 V/Å
Bader charge (|e|)		
C	0.635	0.628

O_1	-0.828	-0.850
O_2(Cu)	-0.844	-0.860
Total on CO_2	-1.032	-1.082
Cu(C)	0.148	0.149
Cu(O_2)	0.242	0.244
Na^+	0.811	0.756
Bond length (Å)		
C-O_1	1.243	1.249
C-O_2	1.341	1.351
C-Cu	1.971	1.974
O_2-Cu	2.082	2.058
O_1-Na	2.245	2.229
O-C-O angle (°)		
	120.9°	119.5°

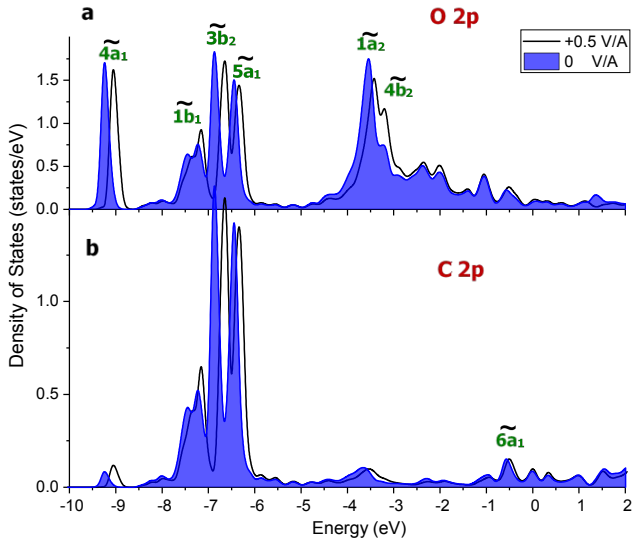

Figure 6. Effect of electric field +0.5 V/Å on projected (**a**) O 2p and (**b**) C 2p and DOS of (CO_2-$Na_{on\ top}$) (**Figure 1b**).

To understand the changes in the $*CO_2^-$ structure by the electric field, we look at the pDOS (**Figure 6**). As predicted earlier,[12,13] all valence orbitals of $*CO_2^-$ are stabilized at 0 vs. +0.5 V/Å, suggesting their stronger hybridization with the metal states. However, the impact of stronger hybridization on the bonding interactions in the system is not straightforward as it

depends on the position of the orbital with respect the Fermi level.[49, 56] Specifically, the LUMO-derived $6\widetilde{a}_1$ orbital crosses the Fermi level with its bonding part (see above). Hence, its stabilization results, apart from attenuation of the C-O bonds of $*CO_2^-$, in an increase in the covalent bonding of $*CO_2^-$ with the surface.

In contrast, the HOMO-derived parallel O-lone pair $4\widetilde{b}_2$ orbital crosses the Fermi level with its antibonding part. Stabilization of such an orbital increases the splitting off antibonding part from the bonding part. As a result, the antibonding part is depopulated and hence the corresponding bonding is strengthened.[49] It follows that the negative electric field stabilizes the Cu-O bond not only through the covalent ($6\widetilde{a}_1$) but also through the dative bonding ($4\widetilde{b}_2$) channel, which can be explained by the synergy between the back-donation and donation to d_{z2} states (see above).

The third situation is realized for the deeper lying molecular orbitals which have fully filled antibonding parts. The net interaction of these orbitals with the metal is the Pauli repulsion.[56] This repulsion increases as the metal surface becomes more negatively charged. The destabilizing effect is expected to be stronger for the C atom due to its closer proximity to the Cu surface (hence a stronger overlap of its occupied orbitals with occupied Cu states) as compared to the O atom. As a result, the Cu-C bond is weakened, while the stabilizing effects dominate in the case of the Cu-O bond. This qualitative result may need further quantitative study.

Conclusions

Using DFT modelling, we demonstrate that the first intermediate of CO_2 electroreduction —carboxylate $*CO_2^-$—is stabilized at the Cu(111)-electrolyte interface by i) the synergy of the covalent and dative bonding, ii) the positive charge on the coordinating Cu atoms and the favorable local electric field generated by a co-adsorbed alkali metal cation, iii) rehybridization of the d states, and iv) rehybridization of the HOMO and LUMO molecular orbitals of $*CO_2^-$. At the electrode-electrolyte interface, even though the alkali cations can be co-adsorbed on the side of $*CO_2^-$, the cation interacts with the carboxylate most strongly when it forms a non-covalent bond (ion pair). For Na^+ as a counter-ion, the most stable structure of this ion pair is hydration-shared. The modelled effect of the external negative electric field reproduces the experimentally observed softening of the C-O and metal-C bonds of $*CO_2^-$. The softening of the metal-C bond can be explained not only by the Stark effect but also by the chemical effects (a more pronounced increase in the Pauli repulsion as compared to the bond stabilization through back-donation). In

addition, our DFT model reveals that the metal-O bond of $*CO_2^-$ is hardened by a negative electric field. This effect is explained by a more pronounced enhancement of the synergetic covalent and dative components of the bond vs. the antagonistic metal-O Pauli repulsion. These results may serve as a stepping-stone towards identifying descriptors of the reaction selectivity toward CO or formate, as well as a basis for a more detailed understanding of the roles of co-adsorbates and hydration on the CO_2 electroreduction.

Conflicts of interest

The authors declare no competing financial interest

Acknowledgements

IC acknowledges the funding support from NSF under award #1336845 and through the I/UCRC Center for Particulate and Surfactant Systems (CPaSS) (IIP-0749461), as well as the financial support from the Department of Geoscience and Petroleum, NTNU, Trondheim. DFT-generated structural images were obtained using VESTA. SP acknowledges the support from Chemical and Petroleum Engineering, Canada First Research Excellence Fund at University of Calgary, and NSERC Discovery grant RGPIN-2016-03851. This research was enabled in part by computational support provided by Compute Canada. The authors also acknowledge communication with Dr. Leanne D. Chen and discussions with Prof. William Goddard, III, Prof. Somasundaran, and Dr. Tao Chen.

References

1. J. Spurgeon and B. Kumar, Energy & Environmental Science, 2018, **11**, 1536-1551
2. M. Bevilacqua, J. Filippi, H. A. Miller and F. Vizza, Energy Technology, 2015, **3**, 197-210.
3. I. V. Chernyshova, P. Somasundaran and S. Ponnurangam, Proceedings of the National Academy of Sciences, 2018, **115**, E9261-E9270.
4. L. D. Chen, M. Urushihara, K. R. Chan and J. K. Norskov, ACS Catalysis, 2016, **6**, 7133-7139.

5. A. Politano, G. Chiarello, G. Benedek, E. V. Chulkov and P. M. Echenique, Surf. Sci. Rep., 2013, **68**, 305-389.
6. L. H. Ou, Y. D. Chen and J. L. Jin, Rsc Advances, 2016, **6**, 67866-67874.
7. J. Onsgaard, J. Storm, S. V. Christensen, J. Nerlov, P. J. Godowski, P. Morgen and D. Batchelor, Surface Science, 1995, **336**, 101-112.
8. H. J. Freund and M. W. Roberts, Surf. Sci. Rep., 1996, **25**, 225-273.
9. J. Onsgaard, L. Thomsen, S. V. Hoffmann and P. J. Godowski, Vacuum, 2006, **81**, 25-31.
10. J. Onsgaard, S. V. Hoffmann, P. Moller, P. J. Godowski, J. B. Wagner, G. Paolucci, A. Baraldi, G. Comelli and A. Groso, Chemphyschem, 2003, **4**, 466-473.
11. J. Onsgaard, L. Bech, C. Svensgaard, P. J. Godowski and S. V. Hoffmann, Progress in Surface Science, 2001, **67**, 205-216.
12. S. Gudmundsdóttir, W. Tang, G. Henkelman, H. Jónsson and E. Skúlason, The Journal of Chemical Physics, 2012, **137**, 164705.
13. K. Bal, S. Huygh, A. Bogaerts and E. Neyts, Plasma Sources Science and Technology, 2018, **27**, 024001.
14. J. Resasco, L. D. Chen, E. Clark, C. Tsai, C. Hahn, T. F. Jaramillo, K. Chan and A. T. Bell, J. Am. Chem. Soc., 2017, **139**, 11277-11287.
15. D. Strmcnik, K. Kodama, D. van der Vliet, J. Greeley, V. R. Stamenkovic and N. M. Markovic, Nature Chemistry, 2009, **1**, 466-472.
16. V. Colic, M. D. Pohl, D. Scieszka and A. S. Bandarenka, Catalysis Today, 2016, **262**, 24-35.
17. S. D. Fried and S. G. Boxer, Accounts of Chemical Research, 2015, **48**, 998-1006.
18. A. Nilsson and L. G. M. Pettersson, in Chemical Bonding at Surfaces and Interfaces, Elsevier, Amsterdam, 2008, DOI: https://doi.org/10.1016/B978-044452837-7.50003-4, pp. 57-142.
19. M. Gajdos, A. Eichler and J. Hafner, Journal of Physics-Condensed Matter, 2004, **16**, 1141-1164.
20. V. A. de la Peña O'Shea, S. González, F. Illas and J. L. G. Fierro, Chemical Physics Letters, 2008, **454**, 262-268.

21. K. Czelej, K. Cwieka and K. J. Kurzydlowski, Catalysis Communications, 2016, **80**, 33-38.
22. S.-G. Wang, X.-Y. Liao, D.-B. Cao, C.-F. Huo, Y.-W. Li, J. Wang and H. Jiao, The Journal of Physical Chemistry C, 2007, **111**, 16934-16940.
23. M. Qiu, Y. Liu, J. Wu, Y. Li, X. Huang, W. K. Chen and Y. F. Zhang, Chinese Journal of Structural Chemistry, 2016, **35**, 669-678.
24. X. J. Liu, L. Sun and W. Q. Deng, Journal of Physical Chemistry C, 2018, **122**, 8306-8314.
25. J. Ko, B.-K. Kim and J. W. Han, The Journal of Physical Chemistry C, 2016, **120**, 3438-3447.
26. X. W. Nie, L. L. Meng, H. Z. Wang, Y. G. Chen, X. W. Guo and C. S. Song, Physical Chemistry Chemical Physics, 2018, **20**, 14694-14707.
27. C. Shi, C. P. O'Grady, A. A. Peterson, H. A. Hansen and J. K. Norskov, Physical Chemistry Chemical Physics, 2013, **15**, 7114-7122.
28. W. An, F. Xu, D. Stacchiola and P. Liu, Chemcatchem, 2015, **7**, 3865-3872.
29. D. A. Lowy and M. Jitaru, in Electrochemically Enabled Sustainability: Devices, Materials and Mechanisms for Energy Conversion, eds. K.-Y. Chan and C.-Y. V. Li, CRC by Taylor&Francis, Boca Raton, 2014, ch. 1, pp. 1-53.
30. G. Kresse and J. Furthmüller, Phys. Rev. B, 1996, **54**, 11169.
31. G. Kresse and J. Furthmüller, Computational Materials Science, 1996, **6**, 15-50.
32. G. Kresse and D. Joubert, Phys. Rev. B, 1999, **59**, 1758.
33. J. P. Perdew, K. Burke and M. Ernzerhof, Physical Review Letters, 1996, **77**, 3865-3868.
34. J. P. Perdew, K. Burke and M. Ernzerhof, Phys. Rev. Lett, 1997, **78**, 1396-1396.
35. G. Henkelman, A. Arnaldsson and H. Jónsson, Computational Materials Science, 2006, **36**, 354-360.
36. W. Tang, E. Sanville and G. Henkelman, J. Phys.: Condens. Matter, 2009, **21**, 084204.
37. S. Sakaki, Bull. Chem. Soc. Jpn., 2015, **88**, 889-938.

38. X. Ding, L. De Rogatis, E. Vesselli, A. Baraldi, G. Comelli, R. Rosei, L. Savio, L. Vattuone, M. Rocca, P. Fornasiero, F. Ancilotto, A. Baldereschi and M. Peressi, Physical Review B, 2007, **76**, 195425
39. M. E. Bjorketun, Z. H. Zeng, R. Ahmed, V. Tripkovic, K. S. Thygesen and J. Rossmeisl, Chemical Physics Letters, 2013, **555**, 145-148.
40. J. Rossmeisl, E. Skulason, M. E. Bjorketun, V. Tripkovic and J. K. Norskov, Chem. Phys. Lett., 2008, **466**, 68-71.
41. S. Schnur and A. Gross, Catalysis Today, 2011, **165**, 129-137.
42. K. Momma and F. Izumi, J. Appl. Crystallogr., 2011, **44**, 1272-1276.
43. W. E. Thompson and M. E. Jacox, The Journal of Chemical Physics, 1999, **111**, 4487-4496.
44. D. H. Gibson, Coordination Chemistry Reviews, 1999, **185-6**, 335-355.
45. F. Flores and J. Ortega, in Molecule-Metal Interface, eds. N. Koch, N. Ueno and A. T. S. Wee, 2013, pp. 17-49.
46. B. Hess and N. F. A. van der Vegt, Proceedings of the National Academy of Sciences of the United States of America, 2009, **106**, 13296-13300.
47. N. F. A. van der Vegt, K. Haldrup, S. Roke, J. R. Zheng, M. Lund and H. J. Bakker, Chemical Reviews, 2016, **116**, 7626-7641.
48. M. Aresta and A. Angelini, in Carbon Dioxide and Organometallics, ed. X. B. Lu, 2016, vol. 53, pp. 1-38.
49. T. Bligaard and J. K. Norskov, in Chemical Bonding at Surfaces and Interfaces, eds. A. Nilsson, L. G. M. Pettersson and J. K. Norskov, 2008, DOI: 10.1016/b978-044452837-7.50005-8, pp. 255-321.
50. T. Schiros, O. Takahashi, K. J. Andersson, H. Ostrom, L. G. M. Pettersson, A. Nilsson and H. Ogasawara, Journal of Chemical Physics, 2010, **132**.
51. N. Mulakaluri, R. Pentcheva and M. Scheffler, Journal of Physical Chemistry C, 2010, **114**, 11148-11156.
52. F. Mittendorfer, A. Garhofer, J. Redinger, J. Klimes, J. Harl and G. Kresse, Physical Review B, 2011, **84**, 4.
53. M. Muller, K. Diller, R. J. Maurer and K. Reuter, Journal of Chemical Physics, 2016, **144**.

54. S. Hedström, E. C. dos Santos, C. Liu, K. Chan, F. Abild-Pedersen and L. G. M. Pettersson, The Journal of Physical Chemistry C, 2018, **122**, 12251-12258.
55. J. H. Chang, A. Huzayyin, K. Lian and F. Dawson, Physical Chemistry Chemical Physics, 2015, **17**, 588-598.
56. O. Karis, J. Hasselstrom, N. Wassdahl, M. Weinelt, A. Nilsson, M. Nyberg, L. G. M. Pettersson, J. Stohr and M. G. Samant, Journal of Chemical Physics, 2000, **112**, 8146-8155.
57. T. Schiros, K. J. Andersson, L. G. M. Pettersson, A. Nilsson and H. Ogasawara, Journal of Electron Spectroscopy and Related Phenomena, 2010, **177**, 85-98.

TOC entry

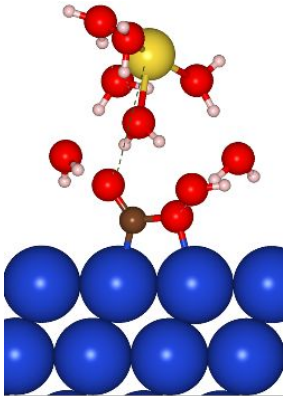

Electric polarization by the local microenvironment strongly affects the CO_2 activation at the electrode-electrolyte interface.